Rainfall estimation from a German-wide commercial microwave link network: Optimized processing and validation for one year of data

Graf Maximilian[1], Chwala Christian[1,2], Polz Julius[1], and Kunstmann Harald[1,2]

[1]Karlsruhe Institute of Technology, Campus Alpin, Institute of Meteorology and Climate Research - Atmospheric Environmental Research, Kreuzeckbahnstr. 19, 82467 Garmisch-Partenkirchen, Germany

[2]University Augsburg, Institute for Geography, Alter Postweg 118, 86159 Augsburg, Germany

Correspondence: Graf Maximilian (maximilian.graf@kit.edu)

Abstract. Rainfall is one of the most important environmental variables. However, it is a challenge to measure it accurately over space and time. During the last decade commercial microwave links (CMLs), operated by mobile network providers, have proven to be an additional source of rainfall information to complement traditional rainfall measurements. In this study we present the processing and evaluation of a German-wide data set of CMLs. This data set was acquired from around 4000 CMLs distributed across Germany with a temporal resolution of one minute. The analyzed period of one year spans from September 2017 to August 2018. We compare and adjust existing processing schemes on this large CML data set. For the crucial step of detecting rain events in the raw attenuation time series, we are able to reduce the amount of miss-classification. This was achieved by a new approach to determine the threshold, which separates a rolling window standard deviation of the CMLs signal into wet and dry periods. For the compensation of wet antenna attenuation, we compare a time-dependent model with a rain-rate-dependent model and show that the rain-rate-dependent model performs better for our data set. As precipitation reference, we use RADOLAN-RW, a gridded gauge-adjusted hourly radar product of the German Meteorological Service (DWD), from which we derive the path-averaged rain rates along each CML path. Our data processing is able to handle CML data across different landscapes and seasons very well. For hourly, monthly and seasonal rainfall sums we found a good agreement between CML-derived rainfall and the reference, except for the winter season with non-liquid precipitation. We discuss performance measures for different subset criteria and show, that CML derived rainfall maps are comparable to the reference. This analysis shows that opportunistic sensing with CMLs yields rainfall information with a good agreement to gauge-adjusted radar data during periods without non-liquid precipitation.

1 Introduction

Measuring precipitation accurately over space and time is challenging due to its high spatiotemporal variability. It is a crucial component of the water cycle and knowledge of the spatiotemporal distribution of precipitation is an important quantity in many applications across meteorology, hydrology, agriculture, and climate research.

Typically, precipitation is measured by rain gauges, ground-based weather radars or spaceborne microwave sensors. Rain gauges measure precipitation at the point scale. Errors can be caused for example by wind, solid precipitation or evaporation losses (Sevruk, 2005). The main disadvantage of rain gauges is their lack of spatial representativeness.

Weather radars overcome this spatial constraint, but are affected by other error sources. They do not directly measure rainfall, but estimate it from related observed quantities, typically via the Z-R relation, which links the radar reflectivity "Z" to the rain rate "R". This relation, however, depends on the rain drop size distribution (DSD), resulting in significant uncertainties. Dual-polarization weather radars reduce these uncertainties, but still struggle with the DSD-dependence of the rain rate estimation (Berne and Krajewski, 2013). Additional error sources can stem from the measurement high above ground, from beam blockage or ground clutter effects.

Satellites can observe large parts of the earth, but their spatial and temporal coverage also has limits. Geostationary satellites can provide a high temporal sampling rate of a specific part of the earth. However rain rate estimates show large uncertainties because they have to be derived from measurements of visible and infra red channels, which were not meant for this purpose. Satellites in Low Earth orbits typically use dedicated sensors for rainfall estimation (microwave radiometers and radars), but their revisiting times are constraint by their orbits. Typical revisit times are in the order of hours to days. As a result, even merged multi-satellite products have a latency of several hours, e.g. the Integrated Multi-satellite Retrievals (IMERG) early run of the Global Precipitation Measurement Mission (GPM) has a latency of 6 hours, while it is limited to a spatial resolution of 0.1 degrees. The employed retrieval algorithms are highly sophisticated and several calibration and correction stages are potential error sources (Maggioni et al., 2016).

Additional rainfall information, for example derived from commercial microwave links (CMLs) maintained by cellular network providers, can be used to compare and complement existing rainfall data sets (Messer et al., 2006). In regions with sparse observation networks, they might even provide unique rainfall information.

The idea to derive rainfall estimates via the opportunistic usage of attenuation data from CML networks emerged over a decade ago independently in Israel (Messer et al., 2006) and the Netherlands (Leijnse et al., 2007). The main research foci in the first decade of dedicated CML research were the development of processing schemes for the rainfall retrieval and the reconstruction of rainfall fields. The first challenge for rainfall estimation from CML data is to distinguish between fluctuations of the raw attenuation data during rainy and dry periods. This was addressed by different approaches which either compared neighbouring CMLs using the spatial correlation of rainfall (Overeem et al., 2016a) or which focused on analyzing the time series of individual CMLs (Chwala et al., 2012; Polz et al., 2019; Schleiss and Berne, 2010; Wang et al., 2012). Another challenge is to estimate and correct the effect of wet antenna attenuation. This effect stems from the attenuation caused by water droplets on the covers of CML antennas, which leads to rainfall overestimation (Fencl et al., 2019; Leijnse et al., 2008; Schleiss et al., 2013).

Since many hydrological applications require spatial rainfall information, several approaches have been developed for the generation of rainfall maps from the path-integrated CML measurements. Kriging was successfully applied to produce countrywide rainfall maps for the Netherlands (Overeem et al., 2016b), representing CML rainfall estimates as synthetic point observation at the center of each CML path. More sophisticated methods can account for the path-integrated nature of the CML observations, using an iterative inverse distance weighting approach (Goldshtein et al., 2009), stochastic reconstruction (Haese et al., 2017) or tomographic algorithms (D'Amico et al., 2016; Zinevich et al., 2010).

CML-derived rainfall products were also used to derive combined rainfall products from various sources (Fencl et al., 2017; Liberman et al., 2014; Trömel et al., 2014). In parallel, first hydrological applications were tested. CML-derived rainfall was used as model input for hydrologic modelling studies for urban drainage modeling with synthetic (Fencl et al., 2013) and real world data (Stransky et al., 2018) or on run-off modeling in natural catchments (Brauer et al., 2016; Smiatek et al., 2017).

With the exception of the research carried out in the Netherlands, where more than two years of data from a country-wide CML network were analyzed (Overeem et al., 2016b), CML processing methods have only been tested on small data sets. We advance the state of the art by performing an analysis of rainfall estimates derived from a German-wide network of close to 4000 CMLs. In this study one CML is counted as the link along one path with typically two sub-links, for the communication in both directions. The temporal resolution of the data set is one minute and the analyzed period is one year from September 2017 until August 2018. The network covers various landscapes from the North German Plain to the Alps in the south, which feature individual precipitation regimes.

The objectives of this study are (1) to compare and adjust selected existing CML data processing schemes for the classification of wet and dry periods and for the compensation of wet antenna attenuation and (2) to validate the derived rain rates with an established rainfall product, namely RADOLAN-RW, both on the country-wide scale of Germany.

2 Data

2.1 Reference data set

The *Radar-Online-Aneichung* data set (RADOLAN-RW) of the German Weather Service (DWD) is a radar-based and gauge adjusted precipitation data set. We use data from the archived real-time product RADOLAN-RW as reference data set throughout this work (DWD). It is a compiled radar composite from 17 dual-polarization weather radars operated by DWD and adjusted by more than 1000 rain gauges in Germany and 200 rain gauges from surrounding countries. RADOLAN-RW does not use dual-pol information, though. It is based on the reflectivity observations in horizontal polarization from each radar site, which are available in real-time every five minutes. This data is then used to compile a national composite of reflectivities, from which rain rates are derived. For the hourly rainfall information of the RADOLAN-RW product, the national composite of 5-minute radar rain rates is then aggregated and adjusted with the hourly rain gauge observations. A weighted mixture of additive and multiplicative corrections is applied. The rain gauges used for the adjustment have a spatial density of approximately one gauge per 300 km^2.

The gridded data set RADOLAN-RW has a spatial resolution of 1 km, covering Germany with 900 by 900 grid cells. The temporal resolution is one hour and the rainfall values are given with a quantization of 0.1 mm. RADOLAN-RW is available with a lag time of around 15 minutes. Detailed information on the RADOLAN processing and products is availabel from DWD (Bartels et al., 2004; Winterrath et al., 2012).

Kneis and Heistermann (2009) and Meissner et al. (2012) compared RADOLAN-RW products to gauge-based data sets for small catchments and found differences in daily, area averaged precipitation sums of up to 50 percent, especially for the winter season. Nevertheless, no data set with comparable temporal and spatial resolution, as well as extensive quality control is available.

In order to compare the path integrated rainfall estimates from CMLs and the gridded RADOLAN-RW product, RADOLAN-RW rain rates are resampled along the individual CML paths. For each CML, the weighted average of all intersecting RADOLAN-RW grid cells is calculated, with the weights being the lengths of the intersecting CML path in each cell. As result, one time series of the hourly rain rate is generated from RADOLAN-RW for each CML. The temporal availability of this reference is 100 percent but we excluded the CML and RADOLAN-RW pairs in the evaluation, when CML data is not available. We chose the RADOLAN-RW product, because it provides both a high temporal and spatial resolution for entire Germany. This resolution is the basis for a good evaluation of the path-averaged rain rates derived from CMLs. The rain gauge adjustments, while not perfect, assures that the RADOLAN-RW rainfall estimates have an increased accuracy compared to a radar-only data set.

2.2 Commercial microwave link data

We present data of 3904 CMLs operated by Ericsson in Germany. Their distribution over Germany is shown in Fig. 1. The CMLs are distributed country-wide over all landscapes in Germany, ranging from the North German Plain to the Alps in the south. The uneven distribution, with large gaps in the north east can be explained by the fact that we only access one subset of all installed CMLs, the Ericsson MINI-LINK Traffic Node systems operated for one cell phone provider.

CML data is retrieved with a real-time data acquisition system which we operate in cooperation with Ericsson (Chwala et al., 2016). Every minute, the current transmitted signal level (TSL) and received signal level (RSL) are requested from more than 4000 CMLs for both ends of each CML. The data is then immediately sent to and stored at our server. For the complete processing chain presented in this work, we used this 1-minute instantaneous data of TSL and RSL for the period from September 2017 to August 2018 for 3904 CMLs to derive rain rates with a temporal resolution of 1 minute. For comparison with the reference data, the 1-minute data is then aggregated. Due to missing, unclear or corrupted metadata we could not use all CML data. Furthermore, we only used data of one sub-link per CML. There was no specific criterion for selecting the sub-link. We simply used the pair of TSL and RSL that came first in our listing.

The available power resolution is 1 dB for TSL and 0.3 (with occasional jumps of 0.4 dB) for RSL. The TSL is constant for 25 percent of the CMLs. An Automatic Transmit Power Control (ATCP), which is able to increase TSL by several dB to prevent blackouts due to heavy attenuation, is active at 75 percent of the CMLs. While the length of the CMLs ranges between a few hundred meters to almost 30 km, most CMLs have a length of 5 to 10 km. They are operated with frequencies ranging from

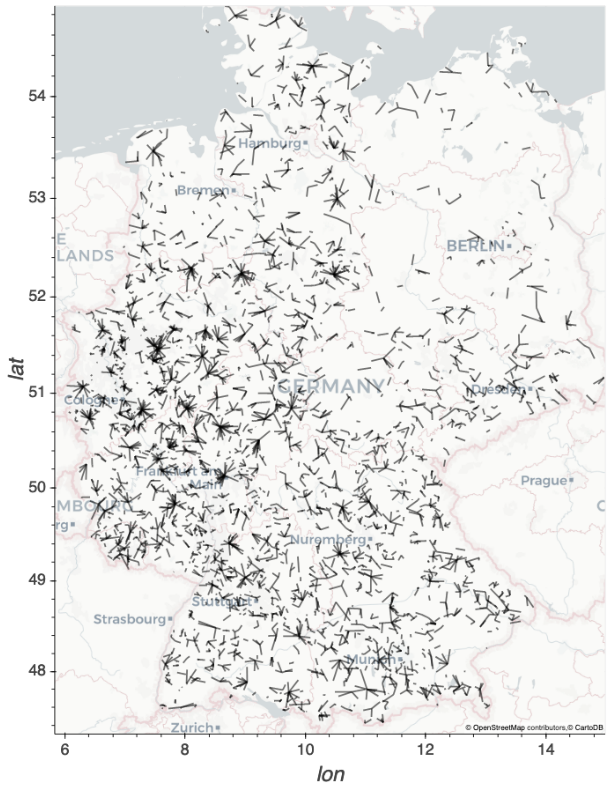

Figure 1. Map of the distribution of 3904 CMLs over Germany. © OpenStreetMap contributors 2019. Distributed under a Creative Commons BY-SA License.

10 to 40 GHz, depending on their length. Figure 2 shows the distributions of path lengths and frequencies. For shorter CMLs higher frequencies are used.

To derive rainfall from CMLs, we used the difference between TSL and RSL, the transmitted minus received signal level (TRSL). An example of a TRSL time series is shown in Fig. 3a). To compare the rain rate derived from CMLs with the reference rain rate, we resampled it from a minutely to an hourly resolution after the processing.

In our CML data set 2.2 percent are missing time steps due to outages of the data acquisition systems. Additionally 1.2 percent of the raw data show missing values (Nan) and 0.1 percent show default fill values (e.g. -99.9 or 255.0) of the CML hardware, which we excluded from the analysis. In order to increase the data availability, we linearly interpolated gaps in raw TRSL time series which were up to five minutes long. This increased the data availability by 0.5 percent. On the one hand, these gaps can be the result of missing time steps and missing values but we also found cases where we suspect very high rainfall to be the reason for short blackouts of a CML.

The size of the complete CML data set is approximately 100 GB in memory. The data set is continuously extended by the operational data acquisition, allowing also the possibility of near-realtime rainfall estimation.

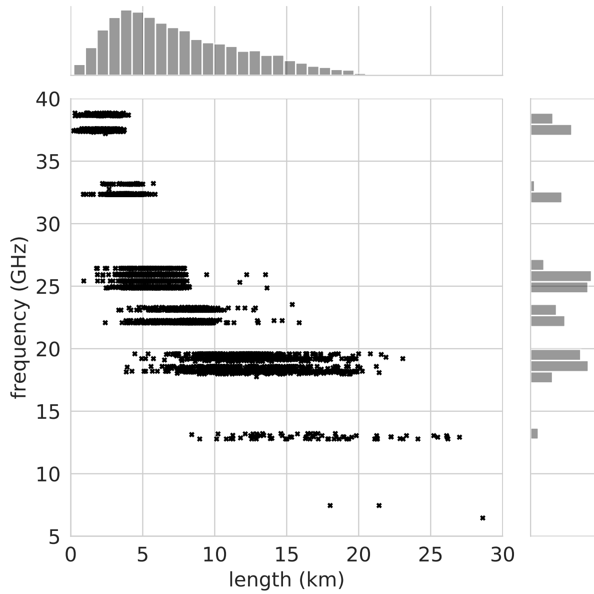

Figure 2. Scatterplot of the length against the microwave frequency of 3904 CMLs including the distribution of length and frequency.

Table 1. Adopted confusion matrix

		reference	
		wet	*dry*
CML	*wet*	true wet (TP)	false wet (FP)
	dry	missed wet (FN)	true dry (TN)

3 Methods

3.1 Performance measures

To evaluate the performance of the CML-derived rain rates against the reference data set, we used several measures which we calculated on an hourly basis. We defined a confusion matrix according to Tab. 1 where *wet* and *dry* refer to hours with and without rain, respectively. The Matthew's correlation coefficient (MCC) summarizes the four values of the confusion matrix in a single measure (1) and is typically used as measure of binary classification in machine learning. This measure is accounting for the skewed ratio of wet and dry events. It is high only if the classifier is performing well on both classes.

$$\mathrm{MCC} = \frac{\mathrm{TP} * \mathrm{TN} - \mathrm{FP} * \mathrm{FN}}{\sqrt{(\mathrm{TP}+\mathrm{FP})(\mathrm{TP}+\mathrm{FN})(\mathrm{TN}+\mathrm{FP})(\mathrm{TN}+\mathrm{FN})}} \tag{1}$$

The mean detection error (MDE) (2) is introduced as a further binary measure focusing on the miss-classification of rain events.

$$\mathrm{MDE} = \frac{\frac{\mathrm{FN}}{\mathrm{n(wet)}} + \frac{\mathrm{FP}}{\mathrm{n(dry)}}}{2} \tag{2}$$

It is calculated as the average of missed wet and false wet rates of the contingency table from Tab. 1.
The linear correlation between CML-derived rainfall and the reference is expressed by the Pearson correlation coefficient (PCC). The coefficient of variation (CV) in (3) gives the distribution of CML rainfall around the reference expressed by the ratio of residual standard deviation and mean reference rainfall,

$$\mathrm{CV} = \frac{\mathrm{std}\sum(\mathrm{R_{CML}} - \mathrm{R_{reference}})}{\overline{\mathrm{R_{reference}}}} \tag{3}$$

where R_{CML} and $R_{\mathrm{reference}}$ are hourly rain rates of the respective data set. Furthermore, we computed the mean absolute error (MAE) and the root mean squared error (RMSE) to measure the accuracy of the CML rainfall estimates. The relative bias is given as

$$\mathrm{bias} = \frac{\overline{(\mathrm{R_{CML}} - \mathrm{R_{reference}})}}{\overline{\mathrm{R_{reference}}}} \tag{4}$$

Often, in studies comparing CML derived rainfall and radar data, a threshold is used as a lower boundary for rainfall. The performance measures, summarized in Tab. 2, were calculated with different subset criteria or thresholds. This gives insight on how CML derived rainfall compares to the reference for different rain rates and on how the large number of data points without rain influence the performance measures. Another reason for listing the performance measures with several thresholds is the increased comparability with other studies on CML rainfall estimation, which do not uniformly use the same threshold, see e.g. Table A1 in de Vos et al. (2019). Therefore, we defined a selection of subset criteria and thresholds and show performance measures for data without any thresholds (*none*), for the data set with R_{CML} and $R_{\mathrm{reference}} < 0.1$ mm/h set to 0 mm/h, for two thresholds where at least R_{CML} or $R_{\mathrm{reference}}$ must be > 0 and >= 0.1 mm/h and two thresholds where $R_{\mathrm{reference}}$ must be >= 0.1 and >= 1 mm.

3.2 From raw signal to rain rate

As CMLs are an opportunistic sensing system rather than part of a dedicated measurement system, data processing has to be done with care. Most of the CML research groups developed their own methods tailored to their needs and data sets. Overviews of these methods are summarized by Chwala and Kunstmann (2019), Messer and Sendik (2015) and Uijlenhoet et al. (2018). The size of our data set is a challenge itself. As TRSL can be attenuated by rain or other sources, described in Sect. 3.2.1 and only raw TSL and RSL data is provided, the large size of the data set is of advantage but also a challenge. Developing and evaluating methods was significantly sped up by the use of an automated processing workflow, which we implemented as a parallelized workflow on a HPC system using the Python packages *xarray* and *dask* for data processing and visual exploration.

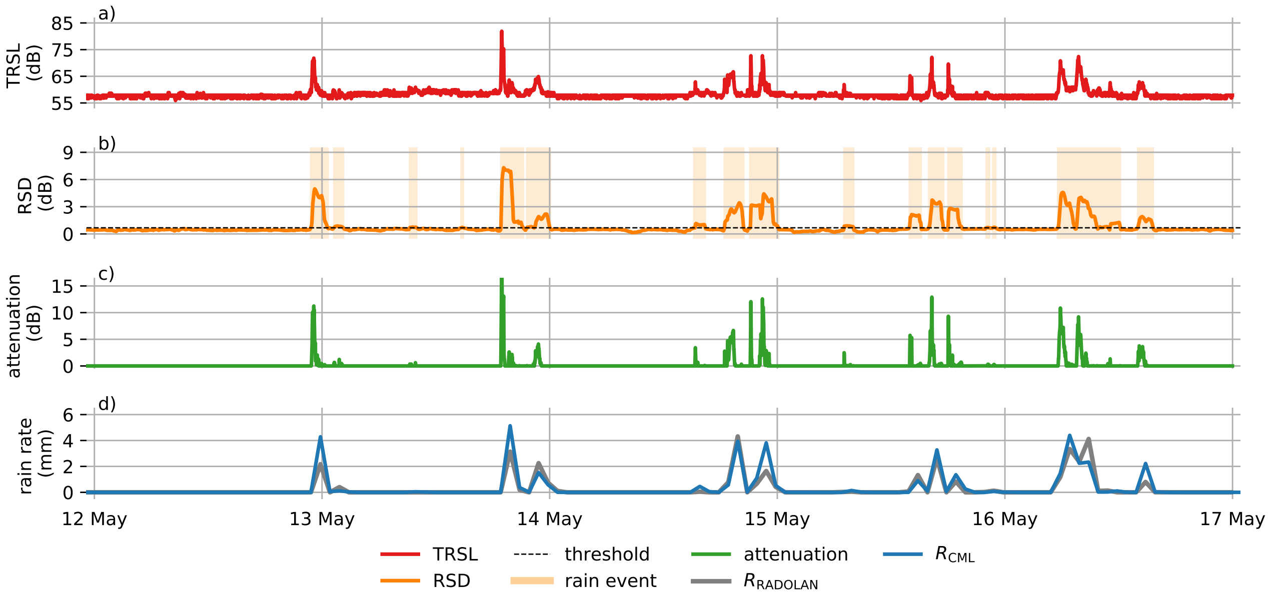

Figure 3. Processing steps from the TRSL to rain rate. a) The TRSL is the difference of TSL - RSL, the raw transmitted and received signal level of a CML. b) The RSD (rolling standard deviation) of the TRSL with an exemplary threshold shows the resulting wet and dry periods. c) The Attenuation is the difference between the baseline and the TRSL during wet periods. d) The derived rain rate is resampled to an hourly scale in order to compare it to the reference RADOLAN-RW.

The major challenges which arose from the processing of raw TRSL data into rain rates and the selected methods from literature are described in the following sections. We use parameters in this processing which are either based on literature, modified from the literature or which we developed in this study. An overview of all used parameters is given in Appendix A1.

3.2.1 Erratic behavior

Rainfall is not the only source of attenuation of microwave radio along a CML path. Additional attenuation can be caused by atmospheric constituents like water vapor or oxygen, but also by refraction, reflection or multi-path propagation of the beam (Upton et al., 2005). In particular, refraction, reflection and multi-path propagation can lead to strong attenuation in the same magnitude as from rain. CMLs that exhibit such behavior have to be omitted due to their noisiness.

We excluded erratic CML data which was extremely noisy or which showed drifts and jumps from our analysis on a monthly basis. To deal with this erratic data, we applied the following sanity checks: We exclude individual CMLs if 1) the five hour moving window standard deviation exceeds the threshold 2.0 for more then ten percent of a month, which typically is the case for CMLs with either a strong diurnal cycle or very noisy periods during a month, or if 2) a one hour moving window standard deviation exceeds the threshold 0.8 more than 33 percent of the time in a month. This filter is based on the approach for detecting rain events in TRSL time series from Schleiss and Berne (2010), which we also use later on in our processing.

For the filter, a fairly high threshold was used, which should only be exceeded for fluctuations stemming from real rain events. The reasoning of our filter is, that if the threshold is exceeded too often, here 33 percent of the time per month, the CML data shows an unreasonably high amount of strong fluctuation. In total, the two sanity checks removed 1.1 percent from our CML data set. Together with the missing values that remain after interpolating data gaps of maximum five minutes in the TRSL time series, 4.2 percent of our data set are not available or not used for processing.

Jumps in data are mainly caused by single default values in the TSL which are described in Sect. 2.2. When we removed these default values, we are able to remove the jumps. TRSL can drift and fluctuate on daily and yearly scale (Chwala and Kunstmann, 2019). We could neglect the influence of these drifts in our analysis, because we dynamically derived a baseline for each rain event, as explained in Sect. 3.2.2. We also excluded CMLs having a constant TRSL over a whole month.

3.2.2 Rain event detection and baseline estimation

The TRSL during dry periods can fluctuate over time due to ambient conditions as mentioned in the previous section. Rainfall produces additional attenuation on top of the dry fluctuation. In order to calculate the attenuation from rainfall, a baseline level of TRSL during each rain event has to be determined. We derived the baseline from the precedent dry period. During the rain event, this baseline was held constant, as no additional information on the evolution of the baseline level is available. The crucial step for deriving the baseline is to separate the TRSL time series into wet and dry periods, because only then the correct reference level before a rain event is used. By subtracting the baseline from TRSL, we derived the attenuation caused by rainfall which is shown in Fig. 3c).

The separation of wet and dry periods is essential, because the errors made in this step will impact the performance of rainfall estimation. Missing rain events will result in rainfall underestimation. False detection of rain events will lead to overestimation. The task of detecting rain events in the TRSL time series is simple for strong rain events, but challenging when the attenuation from rain is approaching the same order of magnitude as the fluctuation of TRSL data during dry conditions.

There are two essential concepts to detect rain events. One compares the TRSL of a certain CML to neighbouring CMLs (Overeem et al., 2016a) and the other investigates the time series of each CML separately (Chwala et al., 2012; Schleiss and Berne, 2010; Wang et al., 2012). We choose the latter one and used a rolling standard deviation (RSD) with a centered moving window of 60 minutes length as a measure for the fluctuation of TRSL as proposed by Schleiss and Berne (2010).

It is assumed that RSD is high during wet periods and low during dry periods. Therefore, an adequate threshold can be defined, which differentiates the RSD time series in wet and dry periods. An example of an RSD time series and a threshold is shown in Fig. 3b) where all data points with RSD values above the threshold are considered as wet.

Schleiss and Berne (2010) proposed the use of a RSD threshold derived from rainfall climatology e.g. from nearby rain gauges. For our data set we assumed that it is raining 5 percent of all minutes in Germany, as proposed by Schleiss and Berne (2010) for their CMLs in France. Therefore, we used the 95 percent quantile of RSD as a threshold, assuming that the 5 percent of highest fluctuation of the TRSL time series refer to the 5 percent of rainy periods. We refer to this threshold as the climatologic threshold. We compared it to two new definitions of thresholds. We are aware that this threshold does not reflect the real climatology at each CML location, nevertheless this method is a rather robust and a simple approach which provides a first rain event detection.

For the first new definition, we derived the optimal threshold for each CML based on our reference data for the month of May 2018. We used the same approach as for the climatologic threshold, but for each CML we tested a range of possible thresholds and calculated the binary measure MCC for each. For each CML we picked the threshold which produced the highest MCC in May 2018 and used it over the whole analysis period.

The second new definition to derive a threshold is based on the quantiles of the RSD, similarly to the climatologic threshold describe above. However, we propose to not focus on the fraction of rainy periods for finding the optimal threshold, since a rainfall climatology is likely not valid for individual years and not easily transferable to different locations. We took the 80th quantile of the RSD of each CML, which can be interpreted as a measure of the strength of the TRSL fluctuation during dry periods, and multiplied it by a constant factor to derive the individual threshold. The 80th quantile can be assumed to be more robust against missclassification than the climatologic threshold, because this quantile represents the general notion of each TRSL time series to fluctuate, rather than the percentage of time in which it is raining. We chose the 80th quantile, since it is very unlikely that it is raining more than 20 percent of the time in a month in Germany.

To find the right factor, we selected the month of May 2018 and fitted a linear regression between the optimal threshold for each CML and the 80th quantile. The optimal threshold was derived beforehand with a MCC optimization from the reference. We then used this factor for all other months in our analysis. Additional, we found it to be similar for all months of the analyzed period.

3.2.3 Wet antenna attenuation

Wet antenna attenuation is the attenuation caused by water on the cover of a CML antenna. With this additional attenuation, the derived rain rate overestimates the true rain rate (Schleiss et al., 2013; Zinevich et al., 2010). The estimation of WAA is complex, as it is influenced by partially unknown factors, e.g. the material of the antenna cover. van Leth et al. (2018) found differences in WAA magnitude and temporal dynamics due to different sizes and shapes of the water droplets on hydrophobic and normal antenna cover materials. Another unknown factor for the determination of WAA is the information whether both, one or none of the antennas of a CML is wetted during a rain event. We selected and compared two parametric WAA correction schemes which do not rely on the use of auxiliary data like near-by rain gauges.

Schleiss et al. (2013) measured the magnitude and dynamics of WAA with one CML in Switzerland and derived a time-dependent WAA model. In this model, WAA increases at the beginning of a rain event to a defined maximum in a defined amount of time. From the end of the rain event on, WAA decreases again, as the wetted antenna is drying off. We ran this scheme with the proposed 2.3 dB of maximal WAA for both antennas together. This is also similar to the WAA correction value of 2.15 dB, which Overeem et al. (2016b) derived over a 12-day period in their data set. For τ, which determines the increase rate with time we chose 15 minutes. The decrease of WAA after a rain event is not explicitly modelled, because this WAA scheme is only applied for time steps, which are considered wet from the rain event detection, which has to be carried out in a previous step.

Leijnse et al. (2008) proposed a physical approach where the WAA depends on the microwave frequency, the antenna cover properties (thickness and refractive index) and the rain rate. A homogeneous water film is assumed on the antenna, with its thickness having a power law dependence on the rain rate. Higher rain rates cause a thicker water film and hence higher WAA. A factor γ scales the thickness of the water film on the cover and a factor δ determines the non-linearity of the relation between rain rate and water film thickness. We adjusted the thickness of the antenna cover to 4.1 mm which we measured from one antenna provided by Ericsson. We are aware of the fact, that antenna covers have different thicknesses. But since we do not have this information for the actual antennas that are used by the CMLs of our data, we use this value, as the best one available. We further adjusted γ to 1.47E-5 and δ to 0.36 in such a way, that the increase of WAA with rain rates is less steep for small rain rates compared to the originally proposed parameters. The original set of parameters suppressed small rain events too much because the WAA compensation attributed all attenuation in the TRSL to WAA. For strong rain events (>10 mm/h), the maximum WAA that is reached with our set of parameters is in the same range as the 2.3 dB used as maximum in the approach of Schleiss et al. (2013).

We want to note that several recent methods quantifying the WAA were developed using auxiliary information such as rain gauge data. This is the reason we did not consider these approaches, as we wanted our CML data processing to be as applicable to new regions as possible. The transferability of WAA estimation methods remains an open scientific question, though. Fencl et al. (2019) quantified the influence of WAA for eight very short (length < 500 m) CMLs using cumulative distribution functions from attenuation and rain gauge data. Their approach is not applicable to new CMLs as it requires calibration for each individual CML based on the local rainfall and attenuation statistics. Ostrometzky et al. (2018) used a rain gauge to estimate the WAA of an E-band CML. They calculated both the (dry, constant during rain events) baseline and the theoretical attenuation using rain gauge data and attributed the residual attenuation as WAA. Moroder et al. (2020) developed a model based on the dynamic antenna parameters reflectivity, efficiency and directivity based on a full-wave simulation and applied it on a dedicated experimental setup with CML antennas (Moroder et al., 2019). To apply this method it is required to continuously collect the individual properties of the CML antennas, which might only be possible in future CML hardware generations.

3.2.4 Derivation of rain rates

The estimation technique of rainfall from the WAA-corrected attenuation is based on the well known relation between specific path attenuation k in dB/km and rain rate R in mm/h

$$k = aR^b \tag{5}$$

with a and b being constants depending on the frequency and polarization of the microwave radiation (Atlas and Ulbrich, 1977). In the currently most commonly used CML frequency range between 15 GHz and 40 GHz, the constants only show a low dependence on the rain drop size distribution. Using the k-R relation, rain rates can be derived from the path integrated attenuation measurements that CMLs provide as shown in Fig. 3 d). We used values for a and b according to ITU-R (2005) which show good agreement with calculations from disdrometer data in southern Germany (Chwala and Kunstmann, 2019, Fig. 3).

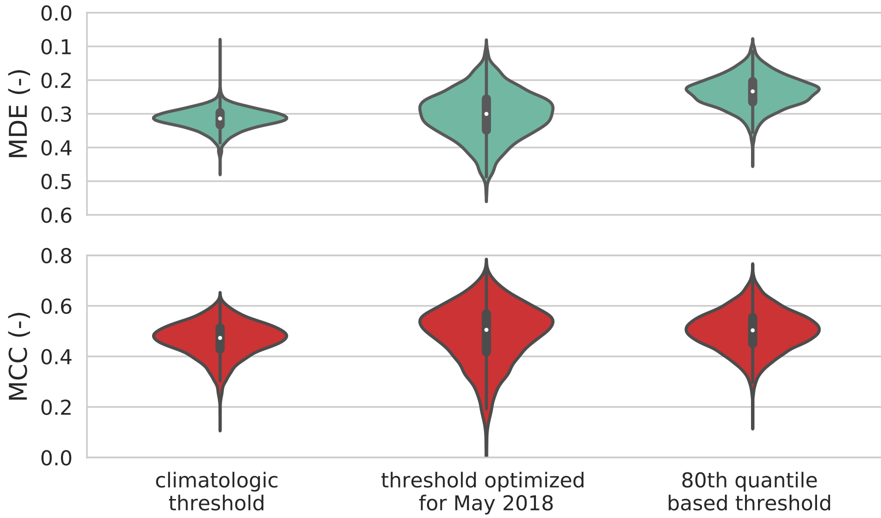

Figure 4. Mean detection error (MDE) and Matthews correlation coefficient (MCC) for three rain event detection schemes for the whole analysis period.

4 Results and Discussion

4.1 Comparison of rain event detection schemes

The separation of wet and dry periods has a crucial impact on the accuracy of the rainfall estimation. We compared an approach from Schleiss and Berne (2010) to three modifications on their success in classifying wet and dry events as explained in Sect. 3.2.2.

The climatologic approach by Schleiss and Berne (2010) worked well for CMLs with moderate noise and when the fraction of times with rainfall over the analyzed periods did correspond to the climatological value. The median MDE was 0.33 and the median MCC of 0.43. The distribution of MDE and MCC values from all CMLs of this climatologic threshold were compared with the performance of the two extensions, displayed in Fig. 4.

When we optimized the threshold for each CML for May 2018 and then applied these thresholds for the whole period, the performance increased with a median MDE of 0.32 and median MCC of 0.46. The better performance of MDE and MCC values highlights the importance of a specific threshold for each individual CML, accounting for their individual notion to fluctuate. The range of MDE and MCC values is wider than with the climatologic threshold, though. The wider range of MDE and MCC values, however, indicates that there is also a need for adjusting the individual thresholds over the course of the year. The 80th quantile-based method had the lowest median MDE with 0.27 and highest median MCC with 0.47. Therefore it miss-classified the least wet and dry periods compared to the other methods.

The threshold, which is based on the 80th quantile, is independent from climatology and depends on the individual notion of a CML to fluctuate. Although the factor used to scale the threshold was derived from comparison to the reference data set as described in Sect. 3.2.2, it was stable over all seasons and for CMLs in different regions of Germany. Validating the scaling factor with other CML data sets could be a promising method for data scarce regions, as no external information is needed.

For single months, the MDE was below 0.20 as shown in Tab. 2, which still leaves room for an improvement of this rain event detection method. Enhancements could be achieved by adding information of nearby CMLs, if available. Also data from geostationary satellite could be used. Schip et al. (2017) found improvements of the rain event detection when using rainfall information from Meteosat Second Generation (MSG) satellite, which carries the Spinning Enhanced Visible and InfraRed Imager (SEVIRI) instrument.

All further processing, presented in the next sections, uses the method based on the 80th quantile.

4.2 Performance of wet antenna attenuation schemes

Two WAA schemes are tested and adopted for the present CML data set. Both are compared to uncorrected CML data and the reference in Fig. 5. Without a correction scheme, the CML-derived rainfall overestimated the reference rainfall by a factor of two when considering mean hourly rain rates, as displayed in Fig. 5a). The correction by Schleiss et al. (2013) produced comparable mean hourly rain rates with regard to the reference data set. Despite its apparent usefulness to compensate for WAA, this scheme worked well only for stronger rain events. The mean detection error is higher than for the uncorrected data set, because small rain events are suppressed completely throughout the year. The discrepancy can also be a result of the path length of 7.6 km in our data set which is four times the length of the CML Schleiss et al. (2013) used. This might have an impact, since shorter CMLs have a higher likeliness that both antennas get wet. Furthermore, the type of antenna and antenna cover impacts the wetting during rain, as discussed in section Sect. 3.2.3.

With the method of Leijnse et al. (2008) the overestimation of the rain rate was also compensated well. It incorporates physical antenna characteristics and, what is more important, depends on the rain rate. The higher the rain rate, the higher the WAA compensation. This leads to less suppression of small events. The MDE is close to the uncorrected data sets and the PCC is higher, as displayed in 5b) and c). Recent results from Fencl et al. (2019) also favor a dynamic, rain intensity depended WAA model, instead of a constant value for WAA compensation. Therefore, the scheme from Leijnse et al. (2008) is used for the evaluation of the CML-derived rain rates in the following sections.

Both methods are parameterized, neglecting known and unknown interactions between WAA and external factors like temperature, humidity, radiation and wind. Current research aims to close this knowledge gap, but the feasibility for large scale networks like the one presented in this study is going to be a challenge as only TSL and RSL are available. A possible solution is the WAA model based on the reflectivityy, efficiency and directivity of the antenna proposed by Moroder et al. (2020), which would have to be measured by future CML hardware. Another approach could be to extend the analysis with meteorological model reanalysis products to be able to better understand WAA behavior in relation to meteorologic parameters like wind, air temperature, humidity and solar radiation.

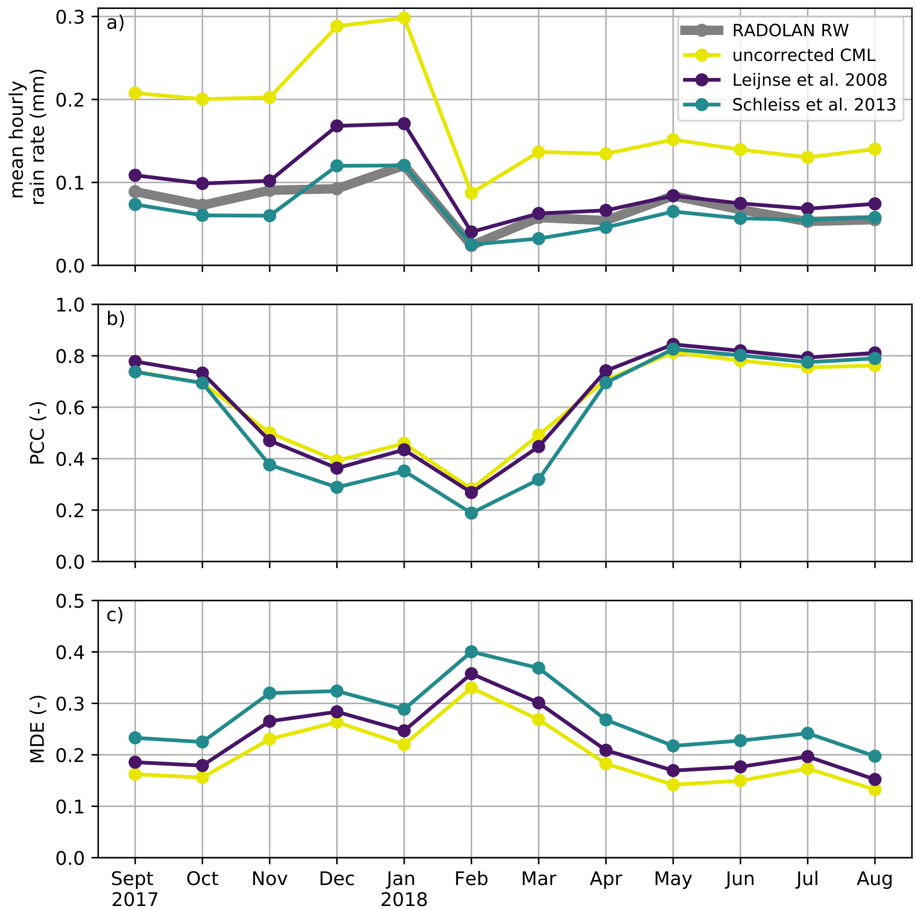

Figure 5. WAA compensation schemes compared on their influence on the a) mean hourly rain rate, b) the correlation between the derived rain rates and the reference and c) the mean detection error between the derived rain rates and the reference.

4.3 Evaluation of CML derived rainfall

Path-averaged rainfall information obtained from almost 4000 CMLs is evaluated against a reference data set, RADOLAN-RW. In Fig. 6 we show scatter density plots of path averaged hourly rain rates, daily rainfall sums and seasonal sums of each CML with the respective performance measures. Furthermore, scatter density plots of hourly, path-averaged rain rates and rain rates from interpolated rainfall maps are compared for each month in Fig. 8 and Fig. 9. Looking at the differences between the seasons in 6, it is evident, that CMLs are prone to produce significant rainfall overestimation during the cold season (DJF). This can be attributed to precipitation events with melting snow, occurring mainly from November to March. Melting snow can potentially cause as much as four times higher attenuation than a comparable amount of liquid precipitation (Paulson and Al-Mreri, 2011). Snow, ice and their melt water on the covers of the antennas can also cause additional attenuation. A decrease of the seasonal performance measures also reflects this effect, as the lowest values for PCC and highest for CV, MAE, RMSE,

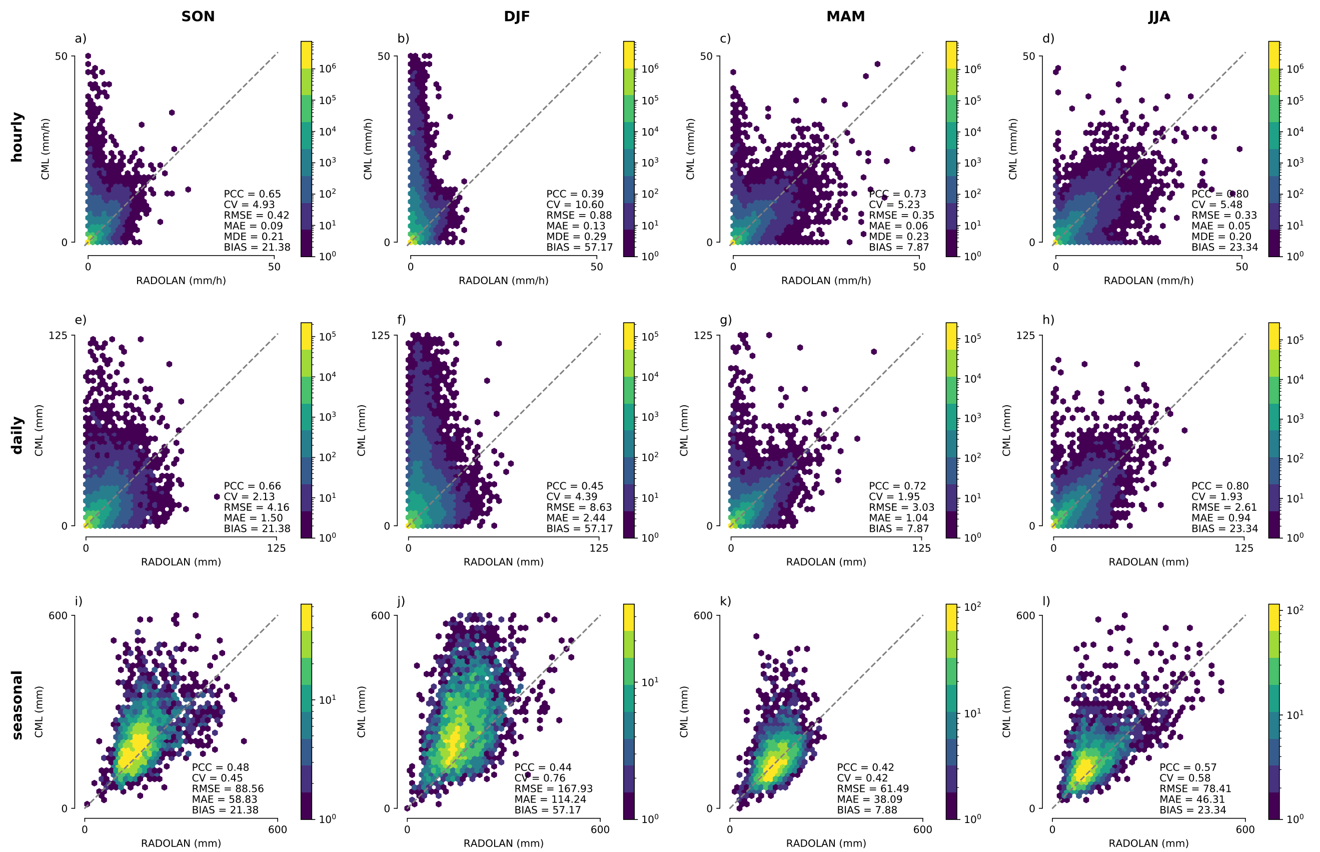

Figure 6. Seasonal scatter density plots of CML-derived rainfall and path-averaged RADOLAN-RW data for hourly, a) - d), daily, e) - h) and seasonal, i) - l) aggregations with respective performance metrics calculated from all available data pairs.

BIAS and MDE are found for DJF. The largest overestimation occurs at low rain rates of the reference. At higher reference rain rates, which most likely are those stemming from liquid precipitation, there is far less overestimation. In spring (MAM) and fall (SON), overestimation by CML rainfall is still visible, but less frequent. This can be explained by the fact, that in the Central German Upland and the Alps, snowfall can occur from October to April. Best agreement between CML-derived rainfall and RADOLAN-RW is found for summer (JJA) months.

The temporal aggregation to daily rainfall sums and the respective performance measures are shown in 6e)-h). The general relation between CML derived rainfall and the reference is similar on both the hourly and daily scale. The BIAS is identical for the daily aggregation. The RMSE and MAE are higher due to the higher rain sums. The overestimation during the winter month is unchanged.

The accumulated rainfall sums of individual CMLs are compared against the reference rainfall accumulation for each season in Fig 6i) - l). The overestimation of the CML derived rainfall sums in DJF, and partly SON and MAM, can again be attributed to the presence of non-liquid precipitation. This overestimation is larger for higher rainfall sums. This could be the result of more extensive snowfall in the mountainous parts of Germany, which are also the areas with highest precipitation year round. Rainfall sums close to zero can be the result from the quality control that we have applied. Periods with missing data in CML time series are consequently not counted in the reference rainfall data set. Therefore, the rainfall sums in Fig. 6 are not representative for the rainfall sum over Germany for the shown period. The PCC for the four seasons shown in Fig. 6i)-l) range from 0.42 in MAM to 0.57 in JJA.

4.4 Performance measures for different subset criteria

Tab. 2 gives an overview of monthly performance measures for different subsets of CML-derived and path-averaged reference rainfall. In the following, we will discuss the effects of the different subset criteria and then compare our results to previous CML rainfall estimation studies.

For all subset criteria, best performance measures are found during late spring, summer and early fall. Highest PCC values are reached when all data pairs, including true dry events, are used to calculate the measures. When very light rain (< 0.1 mm/h) is set to zero on an hourly basis, the performance measures stay very similar, with the exception of CV and BIAS, which show a slight increase in performance. This means that, even when very small rain rates < 0.1 mm are produced, they do not change rainfall sums too much.

When either R_{CML} or $R_{reference}$ have to exceed 0 mm/h, the performance measures are worse than with all data, because all 0 mm/h pairs are removed. When the same subset criterion is set to 0.1 mm/h, a good agreement in the range of very small rain rates below 0.1 mm/h between both data becomes apparent, because the performance measures get worse without them.

To examine the performance of the CML derived rainfall during rain events detected by the reference, two thresholds are selected, where the reference must be above 0.1 and 1 mm/h, respectively, for the period to be considered rainy. With these thresholds, all false wet classifications are removed before the calculation of the performance measures. The PCC with this thresholds is still high for the non-winter months. The CV is reduced, while MAE and RMSE are higher due to higher mean rain rates. The biggest differences can be observed in the bias, where the influence of false wet detection and the overestimation of CMLs over 0.1 and 1 mm/h reduce the bias.

Therefore, when discussing these performance measures in relation to previous studies on CML rainfall estimation, the selection of the threshold is of great importance. de Vos et al. (2019) showed a collection of dutch CML-studies in Table A1. In Tab. 3 we compare our performance measures to those of studies from de Vos et al. (2019) table which are similar to our study. 'Similar' in this context means considering the size and temporal aggregation of the CML data set as well as the use of radar data as a reference for path-averaged (link-based) rain rates from CMLs. The performance measures from our results with the respective thresholds are in the same range as the performance measures from de Vos et al. (2019) and Rios Gaona et al. (2015). The results thus should not be compared in a purely quantitative way, because both use different sampling strategies and span different time periods.

Table 2. Monthly performance measures between path averaged, hourly CML-derived rainfall and RADOLAN-RW as reference for subset criteria and thresholds.

	subset criteria		**2017**				**2018**							
	(mm)	**mean**	**Sept**	**Oct**	**Nov**	**Dec**	**Jan**	**Feb**	**Mar**	**Apr**	**May**	**Jun**	**Jul**	**Aug**
	none	**0.62**	0.78	0.73	0.46	0.36	0.43	0.27	0.45	0.74	0.85	0.81	0.79	0.81
	light rain to 0	**0.62**	0.78	0.73	0.46	0.36	0.43	0.27	0.45	0.74	0.85	0.81	0.79	0.81
PCC	cml or ref > 0	**0.58**	0.74	0.68	0.38	0.28	0.35	0.20	0.37	0.71	0.83	0.80	0.78	0.79
(-)	cml or ref >= 0.1	**0.54**	0.70	0.64	0.34	0.23	0.31	0.13	0.32	0.68	0.81	0.78	0.76	0.77
	ref >= 0.1	**0.58**	0.73	0.71	0.38	0.28	0.35	0.22	0.39	0.73	0.82	0.79	0.80	0.80
	ref >= 1	**0.51**	0.65	0.64	0.32	0.17	0.27	0.12	027	0.67	0.75	0.73	0.73	0.74
	none	**7.01**	3.80	4.40	6.09	11.4	7.62	18.5	6.82	5.20	3.98	5.17	5.88	5.33
	light rain to 0	**7.19**	3.88	4.51	6.23	11.64	7.75	18.28	7.06	5.33	4.03	5.23	5.96	5.40
CV	cml or ref > 0	**3.03**	1.73	2.00	2.96	5.59	3.85	6.82	3.09	2.19	1.60	2.04	2.36	2.10
(-)	cml or ref >= 0.1	**2.42**	1.40	1.64	2.51	4.78	3.35	5.19	2.53	1.67	1.18	1.50	1.71	1.54
	ref >= 0.1	**1.69**	1.05	1.06	1.92	3.61	2.67	3.25	1.90	1.11	0.88	1.01	0.96	0.92
	ref >= 1	**1.11**	0.73	0.69	1.24	2.27	1.73	2.18	1.14	0.70	0.63	0.72	0.67	0.65
	none	**0.08**	0.08	0.08	0.11	0.17	0.17	0.05	0.07	0.05	0.06	0.06	0.05	0.05
	light rain to 0	**0.08**	0.08	0.07	0.11	0.17	0.16	0.05	0.07	0.05	0.05	0.05	0.05	0.05
MAE	cml or ref > 0	**0.41**	0.38	0.36	0.46	0.71	0.64	0.37	0.35	0.30	0.34	0.36	0.33	0.33
(mm/h)	cml or ref >= 0.1	**0.64**	0.58	0.53	0.64	0.97	0.86	0.66	0.53	0.49	0.61	0.64	0.60	0.58
	ref >= 0.1	**0.72**	0.64	0.57	0.70	1.02	0.91	0.68	0.55	0.54	0.73	0.83	0.74	0.69
	ref >= 1	**1.40**	1.16	1.05	1.40	2.02	1.73	1.73	1.25	1.09	1.30	1.51	1.39	1.22
	none	**0.48**	0.34	0.33	0.56	1.08	0.94	0.46	0.41	0.29	0.36	0.35	0.32	0.30
	light rain to 0	**0.48**	0.35	0.33	0.56	1.08	0.94	0.46	0.41	0.29	0.34	0.35	0.32	0.30
RMSE	cml or ref > 0	**1.06**	0.75	0.71	1.16	2.18	1.84	1.25	0.90	0.68	0.84	0.89	0.78	0.75
(mm/h)	cml or ref >= 0.1	**1.34**	0.94	0.87	1.38	2.58	2.14	1.70	1.12	0.90	1.14	1.22	1.08	1.02
	ref >= 0.1	**1.45**	1.01	0.90	1.47	2.66	2.22	1.68	1.15	0.96	1.33	1.52	1.31	1.18
	ref >= 1	**2.33**	1.59	1.43	2.36	4.02	3.33	3.48	1.97	1.61	1.99	2.32	2.04	1.78
	none	**30**	20	34	11	79	39	67	7	21	0	10	30	35
	light rain to 0	**29**	20	34	11	80	40	67	7	20	-2	8	27	32
BIAS	cml or ref > 0	**30**	20	34	11	79	39	67	7	21	0	10	30	35
(%)	cml or ref >= 0.1	**29**	20	33	11	80	40	67	7	20	-2	8	27	32
	ref >= 0.1	**-4**	-1	-1	-15	36	14	-6	-20	-10	-16	-15	-13	-3
	ref >= 1	**-9**	-4	-9	-24	22	2	-16	-21	-12	-15	-17	-13	-5
MDE	none	**0.23**	0.20	0.19	0.24	0.27	0.23	0.35	0.29	0.22	0.19	0.19	0.22	0.17

Table 3. Comparison of the performance measures to similar CML validation studies (only link-based comparisons) with respective thresholds

Study and Dataset	Comparison	Threshold	Bias (%)	CV (-)	PCC (-)
de Vos et al. (2019)					
Average of 1451 CMLs over 7 months (18 Feb–16 Oct 2016), 15 min instantaneously sampled	Link-based comparison with gauge-adjusted radar, 15 min	CML or ref > 0 mm	23	3.43	0.52
Rios Gaona et al. (2015)					
Average of 1514 CMLs over 12 rainy days (June to September 2011), min-max sampled	CML-based comparison with gauge-adjusted ref, 15 min	CML or ref > 0.1 mm	-13	1.44	0.66
This study					
Average of 3904 CMLs over one year (September 2017 - August 2018), one min instantaneously sampled	CML-based comparison with gauge-adjusted radar, hourly	CML or ref > 0 mm CML or ref >= 0.1 mm	30 19	3.03 2.42	0.58 0.54

4.5 Rainfall maps

Interpolated rainfall maps of CML-derived rainfall compared to RADOLAN-RW are shown in Fig. 7, Fig. 8 and Fig. 9. The respective CML maps have been derived using inverse distance weighting (IDW) with the RADOLAN-RW grid as target grid and on an hourly basis. Each CML rainfall value is represented as one synthetic point observation at the center of the CML path. For each pixel of the interpolated rainfall field the nearest 12 synthetic CML observation points are taken into account. Weights decrease with the distance d in km, according to d^{-2}. After the interpolation, we masked out grid cells further away than 30 km from a CML path, for each individual time step. Hence, hourly rainfall maps derived from CMLs are only produced for areas with data coverage. We applied the same mask to the reference data set on an hourly basis to increase the comparability between both data sets. For the aggregated rainfall maps, we summed up the interpolated, individually masked, hourly rainfall fields. As an example, Fig. 7 shows 48 hours of accumulated rainfall in May 2018. The general distribution of CML-derived rainfall reproduces the pattern of the reference very well and the rainfall sums of both data sets are similar. Individual features of the RADOLAN-RW rainfall field are, however, missed due to the limited coverage by CMLs in certain regions. A video of this 48 hour showcase with hourly time steps is published alongside this study (Graf et al., 2020).

A qualitative comparison of monthly aggregation of the hourly rainfall maps is shown in Fig. 8 and Fig. 9. The CML-derived rainfall fields resemble the general patterns of the RADOLAN-RW rainfall fields. Summer months show a better agreement than winter months. This is a direct result of the decreased performance of CML-derived rain rates during the winter season, explained in Sect. 4.3. Strong overestimation is also visible year round for a few individual CMLs, for which the filtering of erratic behavior was not successful.

A quantitative comparison of the CML-derived rainfall maps to the reference is shown in the third column of Fig. 8 and Fig. 9.

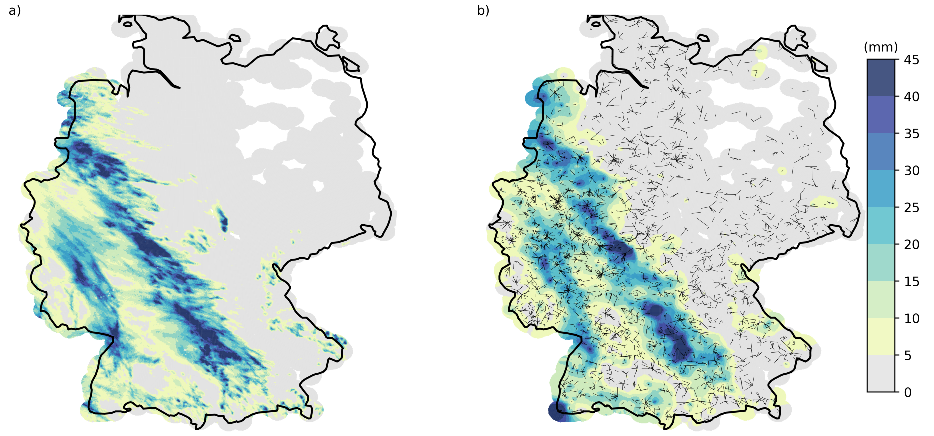

Figure 7. Accumulated rainfall for a 48 hour showcase from 12.05.2018 until 14.05.2018 for a) RADOLAN-RW and b) CML-derived rainfall. CML-derived rainfall is interpolated using a simple inverse distance weighting interpolation. A coverage mask of 30 km around CMLs is used.

For these scatter density plots we used all hourly pixel values of the respective month within the 30 km coverage mask. During the winter month, CMLs show strong overestimation. This is a direct result of non-liquid precipitation as described in Sect. 4.3. From May to August 2018 the reference shows very high rain intensities between 50 and 100 mm/h, which are not produced by the CML rainfall maps. This can be attributed to several reasons. First, CML-derived rainfall, which serves as basis for the interpolation, is path-averaged, with a typical path length in the range of 3-15 km. This means, that the rainfall estimation of a single CML represents an average of several RADOLAN-RW grid cells which smoothes out the extremes. Second, due to the interpolation, rainfall maxima in the CML rainfall maps can only occur at the synthetic observation points at the center of each CML. Third, rainfall is only observed along the path of CMLs and even with almost 4000 CMLs across Germany, the spatial variation of rainfall cannot be fully resolved. In particular in summer, small convective rainfall events might not intersect with CML paths and hence cannot appear in the CML-derived IDW interpolated rainfall fields.

Considering this, the effect of different coverage ranges around the CMLs has to be taken into account. For the map based comparison in Fig. 8 and Fig. 9 we tested several distances from 10 to 50 km. For the presented results we choose 30 km as a trade off between minimizing the uncertainty of the spatial interpolation and the goal to reach country wide coverage with the produced rainfall maps. van de Beek et al. (2012) found an averaged range of around 30 km for summer semi-variograms of 30 years of hourly rain gauge data in the Netherlands, which can be used to justify/enforce our choice. With a 10 km coverage range, the performance measures are better than the ones for 30 km, which are shown in Fig. 8 and Fig. 9. Monthly PCC values show an increase of around 0.05 and the bias is reduced by 3 to 5 percent. Nevertheless, with a coverage of 10 km around the CMLs, coverage gaps emerge not only in the north-eastern part of Germany, but also in the south eastern part. Vice versa, with a 50 km coverage range, the country wide coverage is almost given, while the performance measures are worse compared to 30 km (PCC shows a decrease between 0.03 and 0.05). Overall, the difference of the performance measures of the 10 and 50 km

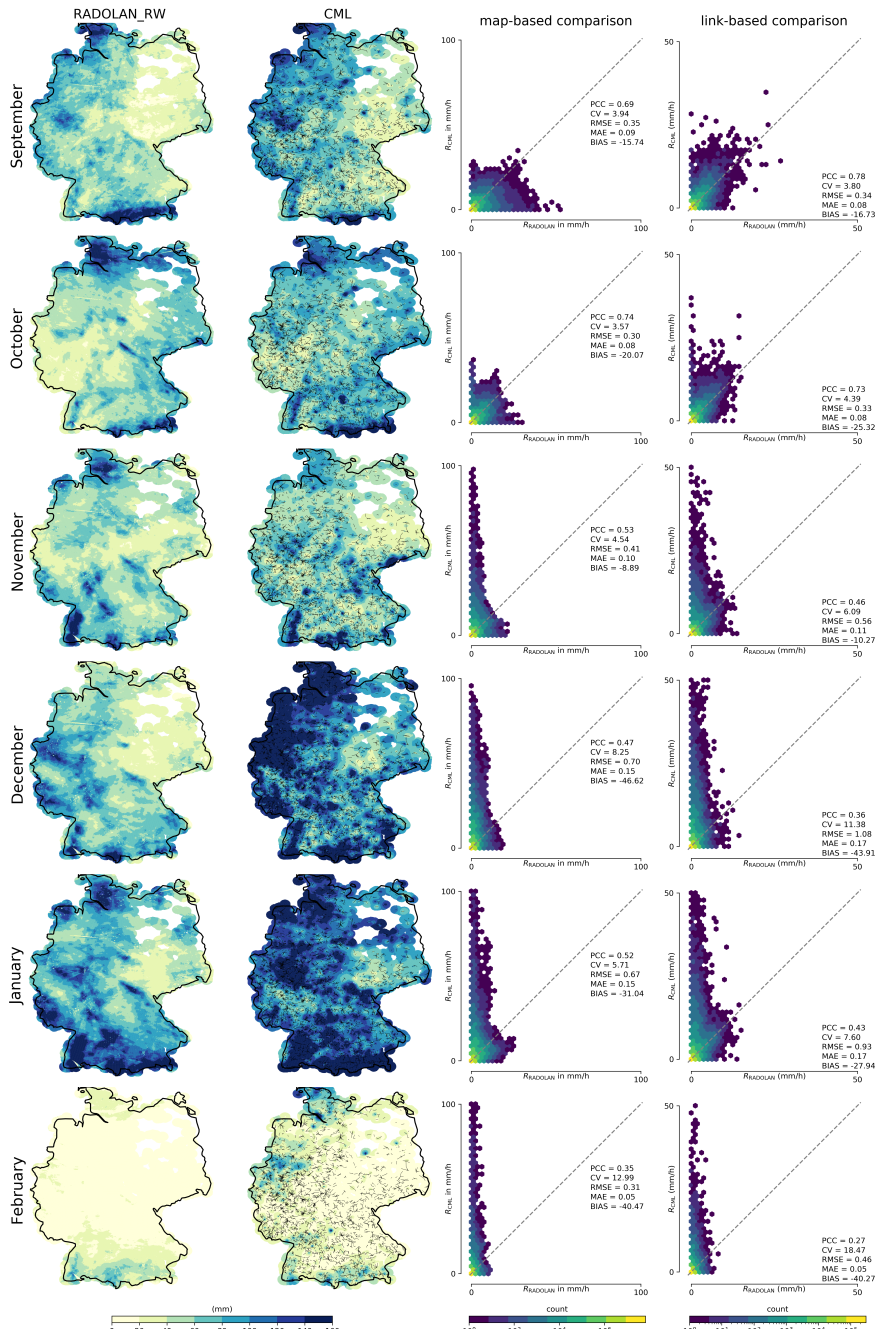

Figure 8. Monthly aggregations of hourly rainfall maps from CMLs compared to RADOLAN-RW from September 2017 until February 2018. For each month two scatter density plots are shown, one for pixel-by-pixel comparison of the hourly maps (map-based comparison), and one for the comparison of the hourly path-averaged rainfall along the individual CMLs (link-based comparison).

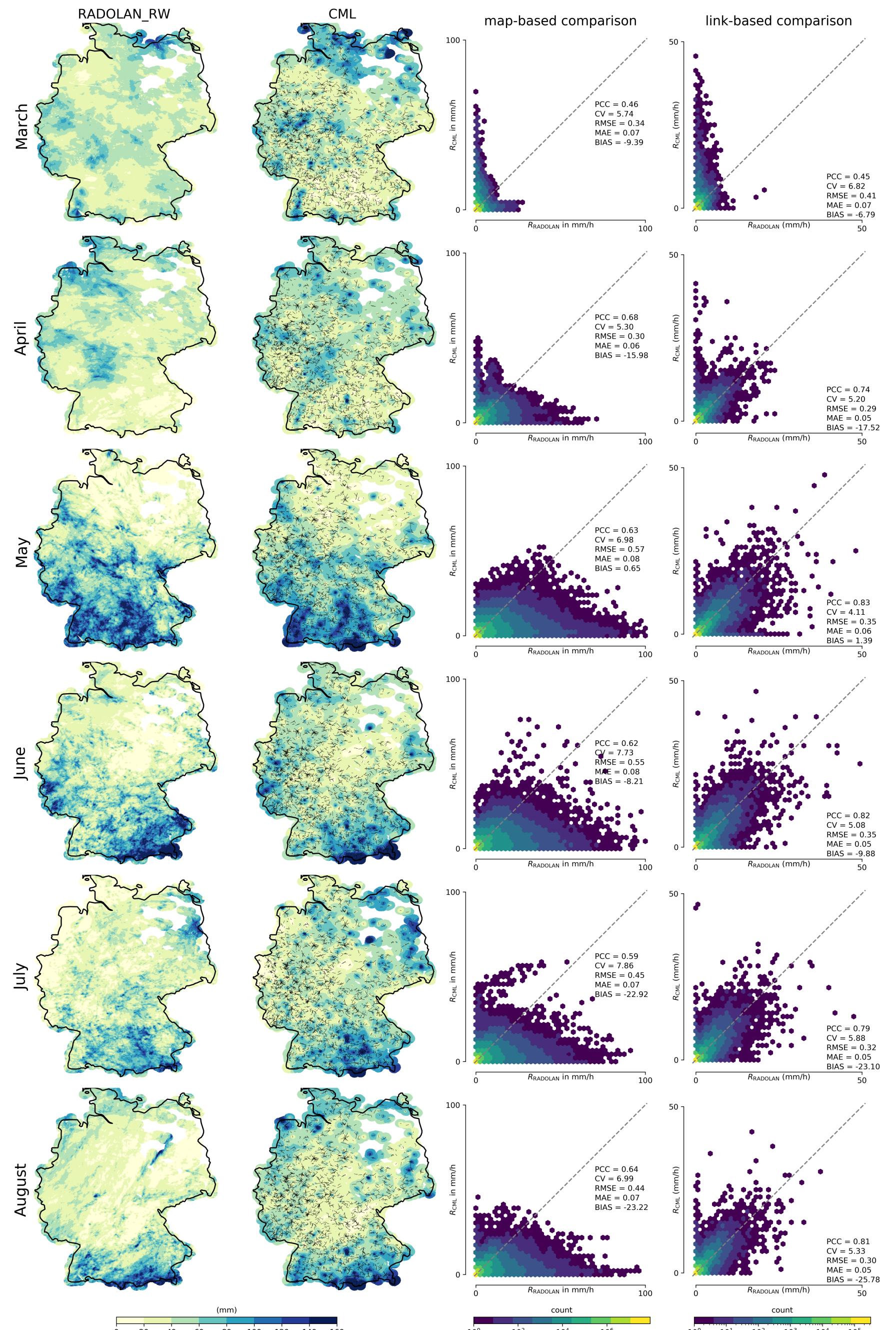

Figure 9. Monthly aggregations of hourly rainfall maps from CMLs compared to RADOLAN-RW from March until August 2018. For each month two scatter density plots are shown, one for pixel-by-pixel comparison of the hourly maps (map-based comparison), and one for the comparison of the hourly path-averaged rainfall along the individual CMLs (link-based comparison).

coverage mask is limited in most parts of Germany by the high density of CMLs, which already lead to an almost full coverage with the 10 km mask.

In order to highlight the differences between a map-based and link-based comparison Fig. 8 and Fig. 9 also show hourly link-based scatter density plots for each month. The differences in the performances measures for the warm months support the qualitative impression, that the map-based comparison perform worse. The interpolation is prone to introduce an underestimation for areas which are more distant to the CML observations. During the winter months, this underestimation compensates the overestimation of the individual CMLs which is due to wet snow and ice covered antennas. Hence, because the two errors compensate each other by chance, this results in slightly better map-based performance measures compared to the link-based measures for the winter months. Nevertheless, rainfall estimation with CMLs for months with non-liquid precipitation is considerably worse than for summer months in all spatial and temporal aggregations.

The derivation of spatial information from the estimated path-averaged rain rates could be improved by applying more sophisticated techniques as described in Sect. 1. We have already carried out several experiments using Kriging, to test one of these potential improvements over IDW. We followed the approach of Overeem et al. (2016b) and adjusted the semivariogram parameters on a monthly basis based on the values from van de Beek et al. (2012). We also tried fixed semivariogram parameters and parameters estimated from the individual CML rainfall estimates for each hour. In conclusion, we, however, only found marginal or no improvements of the performance metrics of the CML rainfall maps. Combined with the drawback of Kriging that the required computation time is significantly increased (approximately 10 to 100 times slower than IDW, depending e.g. on the number of neighboring points used by a moving kriging window), we thus decided to keep using the simple, yet robust and fast IDW interpolation. Furthermore, it is important to note that the errors in rain rate estimation for each CML contribute most to the uncertainty of CML-derived rainfall maps (Rios Gaona et al., 2015). Hence, within the scope of this work, we focused on improving the rainfall estimation at the individual CMLs.

Taking into account that we compare to a reference data set derived from 17 C-band weather radars combined with more than 1000 rain gauges, the similarity with the CML-derived maps, which solely stem from the opportunistic usage of attenuation data, is remarkable.

5 Conclusions

German wide rainfall estimates derived from CML data compared well with RADOLAN-RW, a hourly gridded gauge-adjusted radar product of the DWD. The methods used to process the CML data showed promising results over one year and several thousand CMLs across all landscapes in Germany, except for the winter season.

We presented the data processing of almost 4000 CMLs with a temporal resolution of one minute from September 2017 until August 2018. We developed a parallelized processing work flow, which could handle the size of this large data set. This workflow enabled us to test and compare different processing methods over a large spatiotemporal scale.

A crucial processing step is the rain event detection from the TRSL, the raw attenuation data recorded for each CML. We used a scheme from (Schleiss and Berne, 2010) which uses the 60 minute rolling standard deviation RSD and a threshold.

We derived this threshold from a fixed multiple of the 80th quantile of the RSD distribution of each TRSL. Compared to the original threshold using the 95th quantile, which is based on rainfall climatology, the 80th quantile reflects the general notion of each CML's TRSL to fluctuate. We were able to reduce the amount of miss-classification of wet and dry events, reaching a yearly mean MDE of 0.27, with an average of the MDE for summer months below 0.20. Potential approaches for further decreasing the amount of miss-classifications could be the use of additional data sets. For example, cloud cover information from geostationary satellites could be employed to reduce false wet classification, by, as a first simple approach, defining periods without clouds as dry. Another opportunity would be, to additionally implement algorithms exploiting information of neighboring CMLs.

For the compensation of WAA, the attenuation caused by water droplets on the cover of CML antennas, we compared and adjusted two approaches from literature. In order to evaluate WAA compensation approaches, we used the reference data set. We were able to reduce the overestimation caused by WAA, while maintaining the detection of small rain events, using an adjustment of the approach introduced by Leijnse et al. (2008). The compensation of WAA without an evaluation with a reference data set is not feasible with the CML data set we use.

Compared to the reference data set RADOLAN-RW, the CML-derived rainfall performs well for periods with only liquid precipitation. For winter months, the performance of CML-derived rainfall is limited. Melting snow and snowy or icy antenna covers can cause additional attenuation resulting in overestimation of precipitation, while dry snow cannot be measured at the frequencies and the TRSL quantizations the CMLs in our data set use. We found high correlations for hourly, monthly and seasonal rainfall sums between CML-derived rainfall and the reference. To increase the comparability of our analysis with existing and future studies on CML rainfall estimation we calculated all performance metrics for different subset criteria, e.g. requiring that either CML or reference rainfall is larger than 0 mm.

We found the performance measures of this study to be in accordance with similar CML studies, although the comparability is limited due to differences of the CML and reference data sets. CML-derived rainfall maps calculated with a simple, yet robust inverse distance weighting interpolation showed the plausibility of CMLs as an stand-alone rainfall measurement system.

With the analysis presented in this study, the need for reference data sets in the processing routine of CML data is reduced, so that the opportunistic sensing of country-wide rainfall with CMLs is at a point, where it should be transferable to (reference) data scarce regions. Especially in Africa, where water availability and management are critical, this task should be challenged as Doumounia et al. (2014) did already. The high temporal resolution of the presented data set can be used in future studies, e.g. for urban water management. In addition, CML derived rainfall can also complement other rainfall data sets, e.g. to improve the radar data adjustment in RADOLAN in regions with high CML density and regions, like mountain ranges, where radar data is often compromised. Thus, CMLs can contribute substantially to improve the spatiotemporal estimations of rainfall.

Table A1. Comprehensive overview of used parameters, a short description and their reference from literature if applicable. Parameters with enumeration in parentheses are not used in the final processing.

	description	**parameter value**	**source**
parameters used in final processing routine			
1. Erratic behavior of CMLs (section 3.2.1)			
1.1	sanity check to remove CMLs with strong duirnal cycle or which have noisy periods	5 hour RSD >2 for at lest 10% per month	this study
1.2	sanity check to remove CMLs with high fluctuation over large parts of or the complete month	1 hour RSD >0.8 for at least 33% per month	this study
2. Rain event detection (section 3.2.2)			
2.1	RSD window length	60 min	Schleiss and Berne (2010)
2.2	scaled q80 threshold	1.12 * 80% quantile of RSD	this study
3. WAA compensation (section 3.2.3)			
3.1	thickness of antenna cover	4.1 cm	measured from one antenna cover
3.2	scale for water film thickness γ	1.47E-5	modified after Leijnse et al. (2008)
3.3	factor for the relation between	0.36	modified after Leijnse et al. (2008)
parameters used in alternative processing steps			
(2.3)	climatologic threshold	95% quantile of RSD	Schleiss and Berne (2010)
(3.4)	time for WAA to reach maximum τ	15 min	Schleiss et al. (2013)
(3.5)	maximal value of WAA	2.3 dB	Schleiss et al. (2013)

Code availability. Code used for the processing of CML data can be found in the Python package pycomlink (pycomlink).

Data availability. CML data was provided by Ericsson Germany and is not publicly available. RADOLAN-RW is publicly available through the Climate Data Center of the German Weather Service

6 Appendix A

Author contributions. MG, CC and HK designed the study layout and MG carried it out with contributions of CC and JP. Data was provided by CC. Code was developed by MG with contributions of CC. MG prepared the manuscript with contributions from all co-authors.

Competing interests. The authors declare that they have no conflict of interest.

Acknowledgements. We thank Ericsson for the support and cooperation in the acquisition of the CML data. This work was funded by the Helmholtz Association of German Research Centres within the Project *Digital Earth*. We also like to thank the German Research Foundation for funding the projects *IMAP* and *RealPEP* and the Bundesministerium für Bildung und Forschung for funding the project *HoWa-innovativ*. We further thank the three anonymous reviewers for their valuable comments improving this paper.

References

Atlas, D. and Ulbrich, C. W.: Path- and Area-Integrated Rainfall Measurement by Microwave Attenuation in the 1–3 cm Band, Journal of Applied Meteorology, 16, 1322–1331, https://doi.org/10.1175/1520-0450(1977)016<1322:PAAIRM>2.0.CO;2, https://journals.ametsoc.org/doi/abs/10.1175/1520-0450%281977%29016%3C1322%3APAAIRM%3E2.0.CO%3B2, 1977.

Bartels, H., Weigl, E., Reich, T., Lang, P., Wagner, A., Kohler, O., and Gerlach, N.: Routineverfahren zur Online-Aneichung der Radarniederschlagsdaten mit Hilfe von automatischen Bodenniederschlagsstationen(Ombrometer), Tech. rep., DWD, 2004.

Berne, A. and Krajewski, W. F.: Radar for hydrology: Unfulfilled promise or unrecognized potential?, Advances in Water Resources, 51, 357–366, https://doi.org/10.1016/j.advwatres.2012.05.005, http://www.sciencedirect.com/science/article/pii/S0309170812001157, 2013.

Brauer, C. C., Overeem, A., Leijnse, H., and Uijlenhoet, R.: The effect of differences between rainfall measurement techniques on groundwater and discharge simulations in a lowland catchment, Hydrological Processes, 30, 3885–3900, https://doi.org/10.1002/hyp.10898, https://onlinelibrary.wiley.com/doi/abs/10.1002/hyp.10898, 2016.

Chwala, C. and Kunstmann, H.: Commercial microwave link networks for rainfall observation: Assessment of the current status and future challenges, Wiley Interdisciplinary Reviews: Water, 6, e1337, https://doi.org/10.1002/wat2.1337, https://onlinelibrary.wiley.com/doi/abs/10.1002/wat2.1337, 2019.

Chwala, C., Gmeiner, A., Qiu, W., Hipp, S., Nienaber, D., Siart, U., Eibert, T., Pohl, M., Seltmann, J., Fritz, J., and Kunstmann, H.: Precipitation observation using microwave backhaul links in the alpine and pre-alpine region of Southern Germany, Hydrology and Earth System Sciences, 16, 2647–2661, https://doi.org/https://doi.org/10.5194/hess-16-2647-2012, https://www.hydrol-earth-syst-sci.net/16/2647/2012/hess-16-2647-2012.html, 2012.

Chwala, C., Keis, F., and Kunstmann, H.: Real-time data acquisition of commercial microwave link networks for hydrometeorological applications, Atmospheric Measurement Techniques, 9, 991–999, https://doi.org/10.5194/amt-9-991-2016, https://www.atmos-meas-tech.net/9/991/2016/, 2016.

de Vos, L. W., Overeem, A., Leijnse, H., and Uijlenhoet, R.: Rainfall Estimation Accuracy of a Nationwide Instantaneously Sampling Commercial Microwave Link Network: Error Dependency on Known Characteristics, Journal of Atmospheric and Oceanic Technology, 36, 1267–1283, https://doi.org/10.1175/JTECH-D-18-0197.1, https://journals.ametsoc.org/doi/10.1175/JTECH-D-18-0197.1, 2019.

Doumounia, A., Gosset, M., Cazenave, F., Kacou, M., and Zougmore, F.: Rainfall monitoring based on microwave links from cellular telecommunication networks: First results from a West African test bed, Geophysical Research Letters, 41, 6016–6022, https://doi.org/10.1002/2014GL060724, https://agupubs.onlinelibrary.wiley.com/doi/abs/10.1002/2014GL060724, 2014.

DWD, C. D. C.: Historische stündliche RADOLAN-Raster der Niederschlagshöhe (binär), https://opendata.dwd.de/climate_environment/CDC/grids_germany/hourly/radolan/historical/bin/, version V001.

D'Amico, M., Manzoni, A., and Solazzi, G. L.: Use of Operational Microwave Link Measurements for the Tomographic Reconstruction of 2-D Maps of Accumulated Rainfall, IEEE Geoscience and Remote Sensing Letters, 13, 1827–1831, https://doi.org/10.1109/LGRS.2016.2614326, 2016.

Fencl, M., Rieckermann, J., Schleiss, M., Stránský, D., and Bareš, V.: Assessing the potential of using telecommunication microwave links in urban drainage modelling, Water Science and Technology, 68, 1810–1818, https://doi.org/10.2166/wst.2013.429, /wst/article/68/8/1810/17887/Assessing-the-potential-of-using-telecommunication, 2013.

Fencl, M., Dohnal, M., Rieckermann, J., and Bareš, V.: Gauge-adjusted rainfall estimates from commercial microwave links, Hydrology and Earth System Sciences, 21, 617–634, https://doi.org/https://doi.org/10.5194/hess-21-617-2017, https://www.hydrol-earth-syst-sci.net/21/617/2017/, 2017.

Fencl, M., Valtr, P., Kvičera, M., and Bareš, V.: Quantifying Wet Antenna Attenuation in 38-GHz Commercial Microwave Links of Cellular Backhaul, IEEE Geoscience and Remote Sensing Letters, 16, 514–518, https://doi.org/10.1109/LGRS.2018.2876696, conference Name: IEEE Geoscience and Remote Sensing Letters, 2019.

Goldshtein, O., Messer, H., and Zinevich, A.: Rain Rate Estimation Using Measurements From Commercial Telecommunications Links, IEEE Transactions on Signal Processing, 57, 1616–1625, https://doi.org/10.1109/TSP.2009.2012554, 2009.

Graf, M., Chwala, C., Polz, J., and Kunstmann, H.: Showcase video of hourly RADOLAN and CML rainfall maps, https://doi.org/10.5281/zenodo.3759208, https://zenodo.org/record/3759208, 2020.

Haese, B., Hörning, S., Chwala, C., Bárdossy, A., Schalge, B., and Kunstmann, H.: Stochastic Reconstruction and Interpolation of Precipitation Fields Using Combined Information of Commercial Microwave Links and Rain Gauges, Water Resources Research, 53, 10 740–10 756, https://doi.org/10.1002/2017WR021015, https://agupubs.onlinelibrary.wiley.com/doi/abs/10.1002/2017WR021015, 2017.

ITU-R: Specific attenuation model for rain for use in prediction methods (Recommendation P.838-3). Geneva, Switzerland: ITU-R. Retrieved from https:// www.itu.int/rec/R-REC-P.838-3-200503-I/en, https://www.itu.int/rec/R-REC-P.838-3-200503-I/en, 2005.

Kneis, D. and Heistermann, M.: Bewertung der Güte einer Radar-basierten Niederschlagsschätzung am Beispiel eines kleinen Einzugsgebiets. Hydrologie und Wasserbewirtschaftung, Hydrologie und Wasserbewirtschaftung, 53, 160–171, 2009.

Leijnse, H., Uijlenhoet, R., and Stricker, J. N. M.: Rainfall measurement using radio links from cellular communication networks, Water Resources Research, 43, https://doi.org/10.1029/2006WR005631, https://agupubs.onlinelibrary.wiley.com/doi/abs/10.1029/2006WR005631, 2007.

Leijnse, H., Uijlenhoet, R., and Stricker, J. N. M.: Microwave link rainfall estimation: Effects of link length and frequency, temporal sampling, power resolution, and wet antenna attenuation, Advances in Water Resources, 31, 1481–1493, https://doi.org/10.1016/j.advwatres.2008.03.004, http://www.sciencedirect.com/science/article/pii/S0309170808000535, 2008.

Liberman, Y., Samuels, R., Alpert, P., and Messer, H.: New algorithm for integration between wireless microwave sensor network and radar for improved rainfall measurement and mapping, Atmospheric Measurement Techniques, 7, 3549–3563, https://doi.org/https://doi.org/10.5194/amt-7-3549-2014, https://www.atmos-meas-tech.net/7/3549/2014/, 2014.

Maggioni, V., Meyers, P. C., and Robinson, M. D.: A Review of Merged High-Resolution Satellite Precipitation Product Accuracy during the Tropical Rainfall Measuring Mission (TRMM) Era, Journal of Hydrometeorology, 17, 1101–1117, https://doi.org/10.1175/JHM-D-15-0190.1, https://journals.ametsoc.org/doi/full/10.1175/JHM-D-15-0190.1, 2016.

Meissner, D., Gebauer, S., Schumann, A. H., and Rademacher, S.: Analyse radarbasierter Niederschlagsprodukte als Eingangsdaten verkehrsbezogener Wasserstandsvorhersagen am Rhein, Hydrologie und Wasserbewirtschaftung, 1, https://doi.org/DOI 10.5675/HyWa_2012,1_2, 2012.

Messer, H. and Sendik, O.: A New Approach to Precipitation Monitoring: A critical survey of existing technologies and challenges, IEEE Signal Processing Magazine, 32, 110–122, https://doi.org/10.1109/MSP.2014.2309705, 2015.

Messer, H., Zinevich, A., and Alpert, P.: Environmental Monitoring by Wireless Communication Networks, Science, 312, 713–713, https://doi.org/10.1126/science.1120034, https://science.sciencemag.org/content/312/5774/713, 2006.

Moroder, C., Siart, U., Chwala, C., and Kunstmann, H.: Microwave Instrument for Simultaneous Wet Antenna Attenuation and Precipitation Measurement, IEEE Transactions on Instrumentation and Measurement, pp. 1–1, https://doi.org/10.1109/TIM.2019.2961498, conference Name: IEEE Transactions on Instrumentation and Measurement, 2019.

Moroder, C., Siart, U., Chwala, C., and Kunstmann, H.: Modeling of Wet Antenna Attenuation for Precipitation Estimation From Microwave Links, IEEE Geoscience and Remote Sensing Letters, 17, 386–390, https://doi.org/10.1109/LGRS.2019.2922768, conference Name: IEEE Geoscience and Remote Sensing Letters, 2020.

Ostrometzky, J., Raich, R., Bao, L., Hansryd, J., and Messer, H.: The Wet-Antenna Effect—A Factor to be Considered in Future Communication Networks, IEEE Transactions on Antennas and Propagation, 66, 315–322, https://doi.org/10.1109/TAP.2017.2767620, conference Name: IEEE Transactions on Antennas and Propagation, 2018.

Overeem, A., Leijnse, H., and Uijlenhoet, R.: Retrieval algorithm for rainfall mapping from microwave links in a cellular communication network, Atmospheric Measurement Techniques, 9, 2425–2444, https://doi.org/10.5194/amt-9-2425-2016, https://www.atmos-meas-tech.net/9/2425/2016/, 2016a.

Overeem, A., Leijnse, H., and Uijlenhoet, R.: Two and a half years of country-wide rainfall maps using radio links from commercial cellular telecommunication networks, Water Resources Research, 52, 8039–8065, https://doi.org/10.1002/2016WR019412, https://agupubs.onlinelibrary.wiley.com/doi/abs/10.1002/2016WR019412, 2016b.

Paulson, K. and Al-Mreri, A.: A rain height model to predict fading due to wet snow on terrestrial links, Radio Science, 46, https://doi.org/10.1029/2010RS004555, https://agupubs.onlinelibrary.wiley.com/doi/abs/10.1029/2010RS004555, 2011.

Polz, J., Chwala, C., Graf, M., and Kunstmann, H.: Rain event detection in commercial microwave link attenuation data using convolutional neural networks, Atmospheric Measurement Techniques Discussions, pp. 1–22, https://doi.org/https://doi.org/10.5194/amt-2019-412, https://www.atmos-meas-tech-discuss.net/amt-2019-412/, 2019.

pycomlink: https://github.com/pycomlink/pycomlink.

Rios Gaona, M. F., Overeem, A., Leijnse, H., and Uijlenhoet, R.: Measurement and interpolation uncertainties in rainfall maps from cellular communication networks, Hydrology and Earth System Sciences, 19, 3571–3584, https://doi.org/https://doi.org/10.5194/hess-19-3571-2015, https://www.hydrol-earth-syst-sci.net/19/3571/2015/, 2015.

Schip, T. I. v. h., Overeem, A., Leijnse, H., Uijlenhoet, R., Meirink, J. F., and Delden, A. J. v.: Rainfall measurement using cell phone links: classification of wet and dry periods using geostationary satellites, Hydrological Sciences Journal, 62, 1343–1353, https://doi.org/10.1080/02626667.2017.1329588, https://doi.org/10.1080/02626667.2017.1329588, 2017.

Schleiss, M. and Berne, A.: Identification of Dry and Rainy Periods Using Telecommunication Microwave Links, IEEE Geoscience and Remote Sensing Letters, 7, 611–615, https://doi.org/10.1109/LGRS.2010.2043052, 2010.

Schleiss, M., Rieckermann, J., and Berne, A.: Quantification and Modeling of Wet-Antenna Attenuation for Commercial Microwave Links, IEEE Geoscience and Remote Sensing Letters, 10, 1195–1199, https://doi.org/10.1109/LGRS.2012.2236074, 2013.

Sevruk, B.: Rainfall Measurement: Gauges, in: Encyclopedia of Hydrological Sciences, edited by Anderson, M. G. and McDonnell, J. J., John Wiley & Sons, Ltd, Chichester, UK, https://doi.org/10.1002/0470848944.hsa038, http://doi.wiley.com/10.1002/0470848944.hsa038, 2005.

Smiatek, G., Keis, F., Chwala, C., Fersch, B., and Kunstmann, H.: Potential of commercial microwave link network derived rainfall for river runoff simulations, Environmental Research Letters, 12, 034 026, https://doi.org/10.1088/1748-9326/aa5f46, https://doi.org/10.1088%2F1748-9326%2Faa5f46, 2017.

Stransky, D., Fencl, M., and Bares, V.: Runoff prediction using rainfall data from microwave links: Tabor case study, Water Science and Technology, 2017, 351–359, https://doi.org/10.2166/wst.2018.149, /wst/article/2017/2/351/38782/Runoff-prediction-using-rainfall-data-from, 2018.

Trömel, S., Ziegert, M., Ryzhkov, A. V., Chwala, C., and Simmer, C.: Using Microwave Backhaul Links to Optimize the Performance of Algorithms for Rainfall Estimation and Attenuation Correction, Journal of Atmospheric and Oceanic Technology, 31, 1748–1760, https://doi.org/10.1175/JTECH-D-14-00016.1, https://journals.ametsoc.org/doi/full/10.1175/JTECH-D-14-00016.1, 2014.

Uijlenhoet, R., Overeem, A., and Leijnse, H.: Opportunistic remote sensing of rainfall using microwave links from cellular communication networks, Wiley Interdisciplinary Reviews: Water, 5, https://doi.org/10.1002/wat2.1289, https://onlinelibrary.wiley.com/doi/abs/10.1002/wat2.1289, 2018.

Upton, G., Holt, A., Cummings, R., Rahimi, A., and Goddard, J.: Microwave links: The future for urban rainfall measurement?, Atmospheric Research, 77, 300–312, https://doi.org/10.1016/j.atmosres.2004.10.009, https://linkinghub.elsevier.com/retrieve/pii/S0169809505001079, 2005.

van de Beek, C. Z., Leijnse, H., Torfs, P. J. J. F., and Uijlenhoet, R.: Seasonal semi-variance of Dutch rainfall at hourly to daily scales, Advances in Water Resources, 45, 76–85, https://doi.org/10.1016/j.advwatres.2012.03.023, http://www.sciencedirect.com/science/article/pii/S0309170812000784, 2012.

van Leth, T. C., Overeem, A., Leijnse, H., and Uijlenhoet, R.: A measurement campaign to assess sources of error in microwave link rainfall estimation, Atmospheric Measurement Techniques, 11, 4645–4669, https://doi.org/10.5194/amt-11-4645-2018, https://www.atmos-meas-tech.net/11/4645/2018/, 2018.

Wang, Z., Schleiss, M., Jaffrain, J., Berne, A., and Rieckermann, J.: Using Markov switching models to infer dry and rainy periods from telecommunication microwave link signals, Atmospheric Measurement Techniques, 5, 1847–1859, https://doi.org/https://doi.org/10.5194/amt-5-1847-2012, https://www.atmos-meas-tech.net/5/1847/2012/amt-5-1847-2012.html, 2012.

Winterrath, T., Rosenow, W., and Weigl, E.: On the DWD quantitative precipitation analysis and nowcasting system for real-time application in German flood risk management, IAHS Publ., 351, 7, 2012.

Zinevich, A., Messer, H., and Alpert, P.: Prediction of rainfall intensity measurement errors using commercial microwave communication links, Atmospheric Measurement Techniques, 3, 1385–1402, https://doi.org/10.5194/amt-3-1385-2010, http://www.atmos-meas-tech.net/3/1385/2010/, 2010.